

Anodic Behaviour of Antimony and Antimony-Tin Alloys in Alkaline Solutions

Abd El-Rahman El-Sayed, Ali Mohamed Shaker,* and Hatem Gad El-Kareem

Chemistry Department, Faculty of Science at Sohag, South Valley University, Sohag 82524, Egypt

(Received November 11, 2002)

The electrochemical and corrosive behaviour of antimony and antimony-tin alloys (Alloy No./Sb(wt. %); I/90, II/80, III/65, IV/50) as anodes in various aqueous concentrations of KOH have been investigated using galvanostatic, potentiodynamic and potentiostatic techniques. Galvanostatic potential–time curves at 4 mA cm^{-2} revealed that passivation of both antimony and antimony tin alloys is inhibited by an increase in KOH concentration. The opposite effect was observed with an increase in Sn content in the alloy. At high Sn content and low [OH^-] a pseudo passivation potential was observed. (Abnormal early passivation occurring in the active anodic region due to the formation of tin oxides, which dissolve in alkali. Then, potential decreases.) The alloy with 50% Sn exhibited immediate passivation. The potentiodynamic curves were swept from *E*o.c up to +1000 mV vs SCE. The results showed an increase in the peak current (I_p) for antimony and its alloys with increasing [OH^-] on the oxide film. The first three alloys showed two anodic peaks at −780 and −450 mV, but the forth traced a third peak at −940 mV. X-ray diffraction and SEM micrographs detailed the electrochemical results and morphology of the electrode surface.

There is in the literature the use of antimony as a pH-indicator electrode[1–3] and as an electro-catalyst for electrochemical energy conservation. Antimony is used as an alloying element to harden and mechanically strengthen soft metals such as Sn and Pb. Also, antimony oxide is now an attractive photoconductor but, unfortunately, its resistance is low due to corrosion.[4] There has been little work[5,6] on Sb and Sb-Sn alloys under polarized conditions, especially in alkaline media. Wikstrom and Kennobe[5] studied the kinetics of the electro-oxidation and electro-reduction of Sb in alkaline solutions as well as the electrodeposition of Sb(III) on Sb. Gad Allah et al.[6] reported that under weak oxidation conditions Sb dissolves in the trivalent state as $[Sb(OH)_4]^-$.

In strongly alkaline (above pH 10.4) and in moderate pH solutions, antimony dissolves as $HSbO_2$. The irregular behaviour of the antimony/antimony oxide rest potential has been attributed to the presence of dissolved oxygen.[5] The mechanism of the anodic dissolution of Sb in alkaline solutions has been investigated by many authors.[4,5,7–10] Generally, very little work has been done on the electrochemical behaviour of Sb-Sn alloys in aqueous solutions,[11–13] and no research has been done using potentiodynamic and potentiostatic techniques.

Darwish et al.[11] studied the formation and electrochemical behaviour of some Sn-Sb alloys [(I) 1%, (II) 8.5%, (III) 22%, (IV) 58% and (V) 99% Sb] in various pH media and found that in the pH range 1.4–3.4 the behaviour of the three alloys (I), (II) and (III) showed rather steady and close potential values, indicating a similarity in the electrode reactions, and attributed this to the dissolution of Sn metal in such acidic solutions. Moreover, the local corrosive action is probably induced by the presence of cathodic specks on Sb. Again, the same authors investigated the potential behaviour of some Sn-Sb alloys (1%, 50% and 99% Sb) in buffered phosphate solutions.[13]

In the present work it is intended to elucidate the effect of Sn% in Sb-Sn alloys on the anodic behaviour of Sb in alkaline solutions. Galvanostatic, potentiodynamic and potentiostatic techniques used are complementary and supportive in elucidating the mechanism and behaviour of the anodic polarization of Sb and its alloys.

Experimental

Each solution was prepared by dissolving the appropriate weights of KOH in doubly distilled water. All reagents were of analytical grade. Sb and Sn of high purity (99.999%) were used to prepare both Sb and Sb-Sn alloys as disk electrodes ($A = 0.25$ cm^2) in a Gallenkamp muffle furnace using evacuated closed silica tubes at 950 °C for 24 h. The melts were shaken every 8 h to ensure the homogeneity of melting alloys and quenched in ice to form a solid. Four Sb-Sn alloys were prepared with the following compositions.

The investigated alloys were analyzed using X-ray photoelectron spectroscopy (XPS). For each alloy the percentage of Sb and Sn was found to be in accord with the percentage of Sb and Sn (Table 1). The microhardness of the prepared Sb and Sb-Sn alloys was measured using a Leitz Wetzlar microharness tester with a Vichers-diamond pyramid indicator. A load of 50 g was used, and the microhardness was expressed in Kilograms per square millimeter. X-ray diffraction of the prepared alloys was carried out using a diffractometer with an iron filter and copper radiation was used with an accelerating voltage of 30 kV and a filament current of 20 mA. The morphology of the surface of Sb and Sb-Sn alloys was examined using a scanning electron microscope (JEOL, model 5300).

Table 1. Composition of Four Sb-Sn Alloys

Alloy	I	II	III	IV
Sb (wt %)	90	80	65	50

Published on the web August 15, 2003; DOI 10.1246/bcsj.76.1527

Electrochemical measurements were performed on planar disc electrodes embedded in an Araldite holder. Prior to each measurement the electrodes were polished with successive grades of emery paper degreased in pure ethanol and washed in running bidistillated water before being inserted in to the polarization cell. The reference electrode was a saturated calomel electrode to which all potentials are referred. All the measurements were carried out at 25 °C. The cell description has been given elsewhere.[14]

Galvanostatic measurements were carried out on the Sb and its alloys in different KOH concentrations using a D.C. power supply unit which was connected in series with a large variable resistance. The current density was measured using the apparent surface area of the anode. The potentials were recorded with a digital multimeter (Philips Model PM 2517-X).

Simultaneous potentiodynamic anodic polarization and potentiostatic measurements were carried out by means of a potentiostat/galvanostat (EG&G Model 273) connected with a personal computer (IBM model 30). The potential was altered automatically in the positive direction from the open circuit potential (*E*o.c) up to +1000 mV vs SCE using a scan rate of 1 mV/s controlled by software version 342 C supplied from EG & G Princeton Applied Research.

In some experiments the anodic potential was fixed at a required constant value and the variation of current density was recorded as a function of time (current density–time transients). Details of the experimental procedures have been described elsewhere.[15]

The structure and composition of the passive film formed on the surface of Sb and Sb-Sn anodes in the test solutions were examined using X-ray diffraction and scanning electron microscope (SEM) using the same techniques mentioned before.

Results and Discussion

Mechanical Properties and Composition of Sb and Sb-Sn Alloys. The data in Fig. 1 reveal that the microhardness increases with increasing Sn content in the alloy up to 35% Sn. With a further increase in Sn% in the alloys, the microhardness decreases. The former observed increase in microhardness could be explained by the fact that the addition of Sn to Sb can result in the formation of intermetallic compounds in the solid state.[16] The bonding character of Sb-Sn alloys can be assumed to be mainly metallic. Accordingly, the existence of Sn in a certain content in Sb alloy improves the microhardness properties of Sb. The data of X-ray diffraction, cf. Table 2, showed that alloy Ⅱ (20% Sn) consists of an

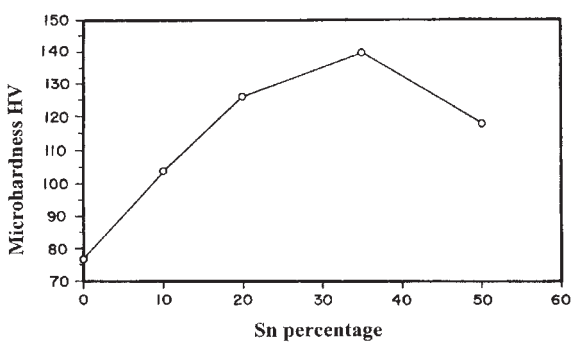

Fig. 1. Variation of microhardness with Sn content in the specimen.

Table 2. X-ray Diffraction Pattern for Alloy Ⅱ (20% Sn)

Experimental values		Reported values		
dA°	I/I°	Sb	Sn	Sb-Sn
3.83	10	3.11	3.75	3.06
3.116	100	2.25	2.29	2.16
3.09	46	1.37	1.96	1.37
2.29	30	2.15	1.48	
2.26	24	1.8		
2.16	23	1.42		
2.14	19	1.37		
1.94	15			
1.77	19			
1.49	5			
1.42	7			
1.38	8			
1.36	4			

Sb-Sn intermetallic structure with the same ratio of the mixture. However, it was observed that some free Sb and Sn coexists in the intermetallic lattice of the Sb-Sn alloy in a separate elemental phase.

Figure 2(a, b, c, d and e) illustrates the surface morphology of different nominal compositions of the system (Sb-Sn) prepared as formerly described. The structure of the Sb sample (Fig. 2a) is composed of a light colored crystalline phase with a laminar structure and a dark amorphous phase. Sb crystallites are imbedded in the amorphous matrix. The two previous phases were observed in the structure of alloy Ⅰ (Fig. 2b), together with plaid-like light grains. The structure of alloy Ⅱ (Fig. 2c) consists of three main phases with different degrees of darkness: a white coloured phase with a laminar structure, dark grains with a polyhedral structure and another dark amorphous phase in which both phases are imbedded. For alloy Ⅲ (Fig. 2d), it appears that the light coloured structure is still dominant. The dark amorphous phase is more pronounced in the structure of alloy Ⅳ (Fig. 2e). Also, the polyhedral dark phase is still present together with the plaid-like dark grains.

Anodic Behaviour of Sb and Sb-Sn Alloys in Alkaline Solution. 1) Galvanostatic Measurements: Figure 3 represents the galvanostatic potential–time curves of Sb and Sb-Sn alloys in 0.2 M KOH solution at a current density of 4 $mA\,cm^{-2}$. These curves all contain the same general features. At the beginning of polarization, the anode remains active for a period of time (except alloy Ⅳ), which depends on the Sn content in the alloy. In the active region, the anode potential rises with time due to oxide growth and the curves exhibit two distinct linear *E-t* relations corresponding to two regions, followed by the evolution of tiny O_2 bubbles. This behaviour can be ascribed to structural changes in the anode film. Interference colors are not observed on Sb anodes in this solution, but the surface has a gray color throughout the measurements. The present results agree with the previous work,[9,12,18] which reported a region of active dissolution of Sb in alkaline solutions before the beginning of passivity. The latter is caused by oxide film formation, which is hindered by high alkali concentration. In the active region of Sb, the anode dissolves continuously according to the following steps:

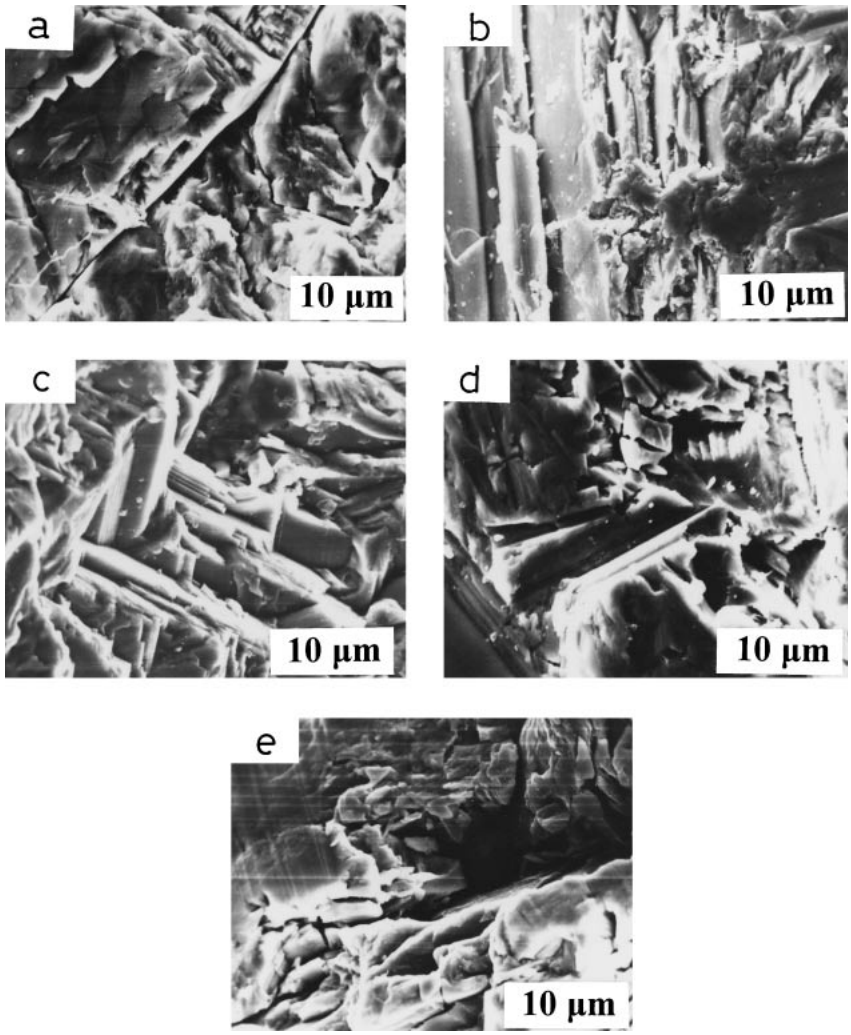

Fig. 2. SEM photographs of the surfaces of (a) Sb, (b) alloy Ⅰ, (c) alloy Ⅱ, (d) alloy Ⅲ and (e) alloy Ⅳ at magnification 2000×.

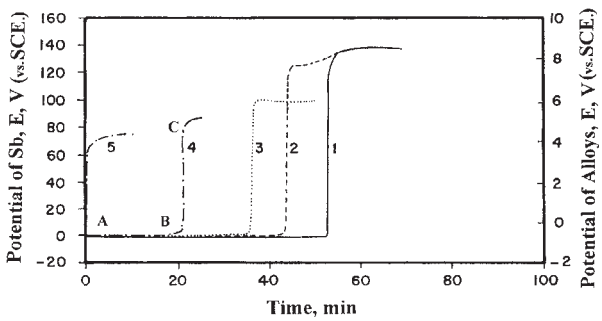

Fig. 3. Anodic potential vs time curves for Sb and its alloys at current density 4 mA/cm^2 in 0.2 M KOH solution. (1) antimony, (2) alloy Ⅰ, (3) alloy Ⅱ, (4) alloy Ⅲ, (5) alloy Ⅳ.

$$Sb + OH^- \rightarrow (SbOH)_{ads.} + e^- \quad (1)$$

$$(SbOH)_{ads.} + OH^- \rightarrow (SbO)_{ads.} + H_2O + e^- \quad (2)$$

$$(SbO)_{ads.} + OH^- \rightarrow HSbO_2 + e^- \quad (3)$$

$$HSbO_2 + OH^- + H_2O \rightarrow [Sb(OH)_4]^- \quad (4)$$

Accordingly, the anode dissolves continuously as $[Sb(OH)_4]^-$ without passivation. Then, the anode potential rises very rapidly at B (active-passive transition) to the inflection potential C, cf. Fig. 3. However, when sufficient oxide has accumulated on the electrode surface, the formation of Sb_2O_3 commences via the following reaction:

$$(SbO)_{ads.} + SbO(OH) + OH^- \rightarrow Sb_2O_3 + H_2O + e^- \quad (5)$$

As soon as, a layer of Sb_2O_3 is formed, the potential rises with time in the anodic direction, and active dissolution of Sb is suppressed. These results indicate that the electrochemical reaction (Eq. 3) is the rate-determining step, which agrees with the reaction reported elsewhere.[17] It is observed that the passivation time increases with increasing concentration of alkali solution up to 0.5 M (Fig. 4). However, no passivation is observed for Sb in 1 M KOH within the allowed time for this experiment. The anodic passivation potential values of Sb reach 200 V in diluted KOH solution.[12] This indicates that a very thick oxide film is formed on the Sb surface. Moreovre, the passivation potential decreases with increasing KOH concentration due to the dissolution of the oxide film.

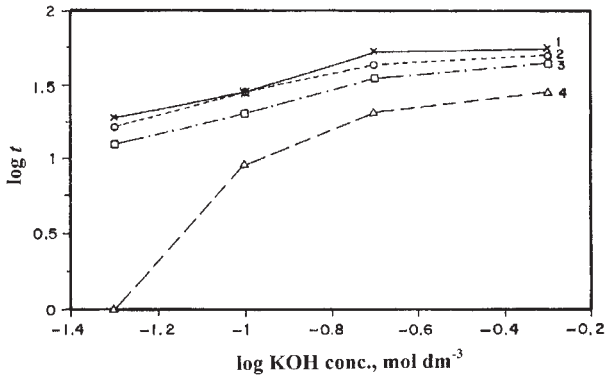

Fig. 4. Dependence of passivation time for (1) Sb (2) alloy I, (3) alloy II and (4) alloy III on the concentration of KOH solution.

Comparison between the curves in Fig. 3 reveals that the anodic passivation potential of Sb reaches 150 V, while for its alloys the maximum passivation potential ranges from 8 to 4.5 V. This indicates that increasing the percentage of Sn content in the Sb-Sn alloy reduces the anodic passivation potential. This behaviour may be attributed to the competition between the processes occurring on Sb and Sn in the alloy.[19] The coexistence of Sn with Sb inhibits the growth of antimony oxides on the electrode surface. However, the behaviour of alloy IV (50% Sn) is different compared to the other investigated three alloys due to the large presence of Sn content in the alloy. The curves in Fig. 3 show that, as the current is switched on, the anodic potential rises very rapidly and almost linearly to an inflection potential at point C, where the permanent passivation occurs. Before the inflection potential C, the polarization curve does not exhibit any potential break, due to the following, thermodynamically possible, reaction:

$$Sn + 4OH^- \rightarrow Sn(OH)_4 + 4e^- \quad (6)$$

The following oxidation reaction may also take place:

$$Sn + 2OH^- \rightarrow Sn(OH)_2 + 2e^- \quad (7)$$

$$Sn(OH)_2 + 2OH^- \rightarrow Sn(OH)_4 + 2e^- \quad (8)$$

The equilibrium potentials of these reactions have been reported elsewhere.[20] Further chemical changes may occur, where some reactions involving dehydration of both $Sn(OH)_2$ and $Sn(OH)_4$ to give SnO and SnO_2, can take place:

$$Sn(OH)_2 \rightarrow SnO + H_2O \quad (9)$$

$$Sn(OH)_4 \rightarrow SnO_2 + 2H_2O \quad (10)$$

Sb in the alloy is also oxidized to form Sb_2O_3 according to the following steps:

$$2Sb + 6OH^- \rightarrow Sb_2O_3 + 3H_2O + 6e^- \quad (11)$$

The product (Sb_2O_3) may be converted into Sb_2O_5 by the surface oxidation under appropriate conditions.[21] It is observed that at higher concentration of KOH (1 M), the dropping potential of this region is characterized by oscillations denoting formation and dissolution of the film on the electrode surface.[14]

Therefore, the addition of Sn to Sb leads to the decrease of the passivation potential and the passivation time (τ). It can be clearly shown that the tendency of the alloys towards passivity increases with increasing Sn content. The dependence of the passivation time on the KOH concentration is shown in Fig. 4 for both Sb and its alloys. It is observed that the corrosive action of KOH solution decreases in the order:

Sb > alloy I > alloy II > alloy III

2) Potentiodynamic Measurements: Figure 5 represents the potentiodynamic polarization curves for Sb and its alloys in 0.2 M KOH solution. The curves were swept from *E*o.c up to the positive potential (+1000 mV vs SCE) with a scan rate of 1 mV s^{-1}. The polarization curves showed an active dissolution peak, permanent passivation and finally a transpassive region. In previous work,[6] the charge transfer reaction occurs in the active dissolution region resulting in the formation of $HSbO_2$, followed by a chemical dissolution to give $[Sb(OH)_4]^-$ ions. Therefore, active dissolution of Sb in the alkaline media takes place.[6] When the formation rate of $HSbO_2$ and/or $(SbO)_{ads.}$ exceeds the dissolution rate, the current drops, indicating the onset of passivation according to reaction (5). Pitman et al.[22] concluded that under weak oxidizing conditions, Sb goes into solution in the trivalent state as $[Sb(OH)_4]^-$ in strongly alkaline solutions (above pH = 10.4). However, the peak potential of Sb in 0.2 M KOH solution (pH = 12.8) appeared at about −420 mV vs SCE. This peak potential approximately represents the equilibrium potential of Sb_2O_3/Sb_2O_5 (mixed oxides) according to the following equation:

$$E = E^{o}_{Sb_2O_3/Sb_2O_5} - 0.059pH \quad (12)$$

The peak potential value calculated from this equation is equal to −325 mV vs SCE, which is 95 mV more positive than the observed value(−420 mV). The latter negative shift (early oxide film formation) may be attributed to the presence of oxide at the electrode surface before measurements due to exposure of the surface to air. However, Sb_2O_3 may be predominantly formed at this peak potential together with a small amount of Sb_2O_5. This suggestion is supported by X-ray diffraction, which will be discussed later. The permanent passivation region extends over a potential range with decreasing current density until it reaches a very small current value (al-

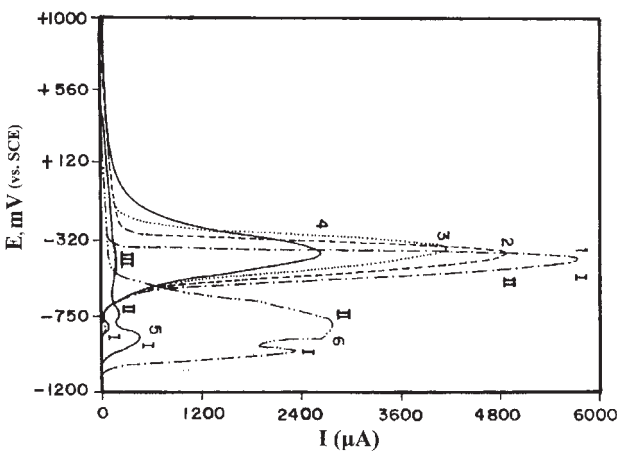

Fig. 5. Potentiodynamic curves for: (1) antimony, (2) alloy I, (3) alloy II, (4) alloy III, (5) alloy IV and (6) tin.

most zero) flowing along the permanent passivation that may be corresponding to the oxide film thickening and repairing of the chemically dissolved film material.[23] Grube et al.[7] stated that the SbO_2^- ion readily absorbs oxygen from the air. This excess oxygen in the solution in contact with the metal would support the formation of Sb_2O_3 and Sb_2O_5. A similar behaviour in the first three investigated alloys to that exhibited by Sb the anode was observed. However, a very small peak potential is obtained at about −800 mV vs SCE (close to the starting anodizing polarization#), in addition to that formed at −400 mV. The current value of this small peak increases as the Sn content in the alloy is increased. The very small anodic current peak of the first three investigated alloys can be attributed to the oxidation of Sn to SnO_2 (Sn/SnO_2 or $Sn/Sn(OH)_4$) according to the following reaction:

$$Sn + 4OH^- \rightarrow Sn(OH)_4 + 4e^- \quad (13)$$

The second anodic peak was observed at −460 mV vs SCE, indicating that the formation of Sb_2O_3 is followed by the formation of Sb_2O_5.

Alloy (Ⅳ) exhibited different behaviour compared to the first three alloys, which may be due to the high percentage of Sn in the alloy. The curve of alloy (Ⅳ) showed three peaks. The first at potential about −940 mV, the second at −720 mV and the third at −440 mV vs SCE. However, the data reveal that the anodic current of peak I is much higher than that of peaks Ⅱ and Ⅲ. From the literature,[21] the charge transfer reaction occurs in the primary active dissolution region resulting in the formation of Sn(Ⅱ) according to reaction (7).

Dehydration of this hydroxide may take place to give SnO, followed by chemical dissolution to give stannite $HSnO_2^-$ ions:

$$Sn(OH)_2 + OH^- \rightarrow HSnO_2^- + H_2O \quad (14)$$

$$SnO + OH^- \rightarrow HSnO_2^- \quad (15)$$

Furthermore, complicated species such as $[Sn(OH)_4]^{2-}$ and $[Sn(OH)_6]^{4-}$ may be formed as soluble products, or in other words, an active dissolution of Sn in the alkaline media may take place.[24,25] When the rate of $Sn(OH)_2$ and/or SnO formation exceeds that of its dissolution, the current drops, indicating the onset of the primary passivation at a potential comparable with the equilibrium potential of $Sn/Sn(OH)_2$ and/or Sn/SnO systems (The difference in potential between the two systems is very small $\simeq$ 12 mV).[20] Therefore, the primary passivation is established as a dissolution–precipitation mechanism. Stirrup et al.[26] adopted the opinion that the active dissolution to form $HSnO_2^-$ is the main feature of this region. The dissolution goes on until the solubility limit of $HSnO_2^-$ at the anode surface is exceeded and precipitation of $Sn(OH)_2$ and/or SnO has started. During the second dissolution region, both $Sn(OH)_2$ and SnO may undergo further oxidation to give $Sn(OH)_4$, according to reaction (8).

$$SnO + 2OH^- + H_2O \rightarrow Sn(OH)_4 + 2e^- \quad (16)$$

$$E = -0.740 - 0.059 \log [OH^-] \quad (17)$$

is the earliest potential (usually the highest negative) at which anodic dissolution occurs.

The observed peak Ⅲ corresponds, approximately, to that of Sb_2O_3/Sb_2O_5 (mixed oxides). The potential value of peak Ⅲ in KOH solution is found to be 40 mV more negative than the equilibrium potential of the system Sb_2O_3/Sb_2O_5 in the corresponding pH of the solution. This negative shift is probably due to the existence of both Sb/Sb_2O_3 and Sb_2O_3/Sb_2O_5 systems and this potential value can be considered to be a mixed potential involving both systems. Comparing the potentiodynamic polarization curves (Fig. 5) of Sb, Sn and Sb-Sn alloys, it is observed that the peak current of Sb is higher than that of Sn. However, for Sb-Sn alloys, the current peak gradually decreases with increasing Sn content in the alloy compared with the current peak of Sb. In the case of alloy (Ⅳ) (50% Sn), the current peaks Ⅱ and Ⅲ are very small compared with the peaks of both Sn and Sb metals. This behaviour suggests that the Sn content in the Sb-Sn alloy plays an important role in decreasing the corrosion rate of Sb in alkaline solution. For the alloy electrodes, the increase in Sn content from 10% to 50% decreases the anodic corrosion current of the alloy under the same conditions, improving its stability against corrosion. This behaviour indicates a beneficial effect of Sn content in the alloy.

Curves in Fig. 6 show that increasing the concentration of KOH enhances the anodic current peak (related to Sb_2O_3/Sb_2O_5) in the case of both Sb and its investigated alloys. Logarithmic straight line relations were obtained, and the current peak gradually decreased with increasing Sn content in the alloy. These results, together with those obtained by the galvanostatic technique, assume that the alloy surface is well protected, most probably by slightly porous anodically formed films of mixed oxides (SnO_2, Sb_2O_3 and Sb_2O_5).[21]

3) Potentiostatic Measurements: Figures 7 and 8 show a comparison between the potentiostatic measurements for Sb and Sb-Sn alloys at the active dissolution peak (−400 mV vs SCE) on one hand and the transpassive region (+1000 mV vs SCE) on the other hand. The curves can be divided into four stages. The first stage corresponds to the current decay to a minimum. The second stage involves an increase in the anodic current value to a maximum. Then, the current density decreases steeply (third stage) to a steady-state value, which represents the fourth stage. These findings demonstrate that the first stage for Sb, corresponding to the current decay, may be due to the formation of $HSbO_2$ molecules on the elec-

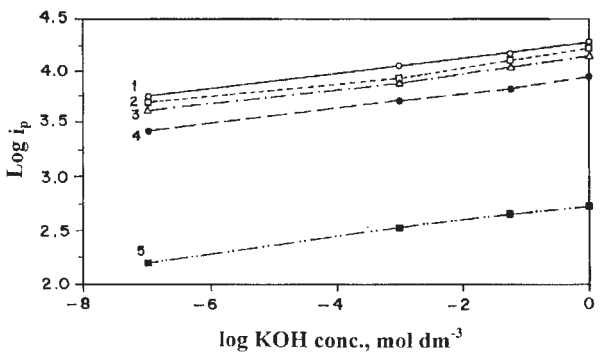

Fig. 6. Dependence of the anodic current peaks of (1) Sb; (2) alloy I; (3) alloy Ⅱ; (4) alloy Ⅲ and (5) alloy Ⅳ on the concentration of KOH solution.

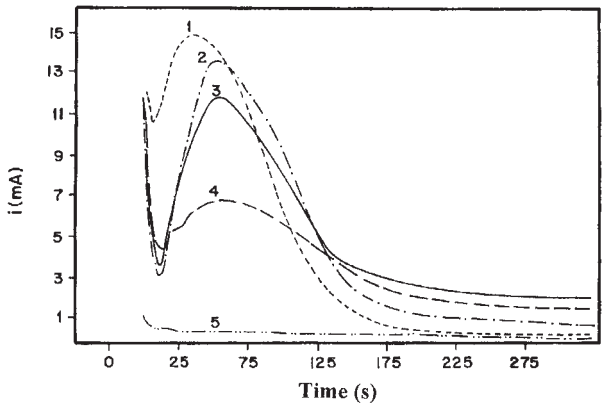

Fig. 7. Comparison between potentiostatic transients current vs time curves for Sb and its Sb-Sn alloys in 0.2 M KOH solution at applied potential −400 mV. Curve: (1) antimony, (2) alloy Ⅰ, (3) alloy Ⅱ, (4) alloy Ⅲ, (5) alloy Ⅳ.

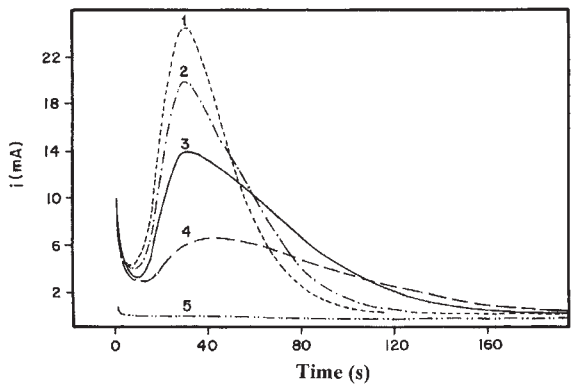

Fig. 8. Comparison between potentiostatic transients current vs time curves for Sb and its Sb-Sn alloys in 0.2 M KOH solution at applied potential +1000 mV. Curve: (1) antimony, (2) alloy Ⅰ, (3) alloy Ⅱ, (4) alloy Ⅲ, (5) alloy Ⅳ.

trode surface.[6] The dissolution of $HSbO_2$ molecules in strong alkaline solutions, giving $Sb(OH)_4^-$, leads to an increase in the current-density to a maximum (second stage). The observed steep decay of the current density results when sufficient oxide, Sb_2O_3, has accumulated on the surface (third stage). As the degree of the electrode surface coverage with the porous Sb_2O_3 oxide layer increases, the true current density at the bare surface increases, leading to the higher oxidation state oxide, Sb_2O_5, formed on the electrode surface. Thus, a very thick oxide film is formed on the surface.

The observed decrease in steady-state current density values, with increasing applied potential, is due to the surface coverage with more oxides (the data not represented in the text).

4) Composition of the Passive Film: The composition of the passive film formed on the surfaces of Sb and alloy Ⅱ (20% Sn) after anodic potentiostatic polarization treatment in 0.2 M KOH solution for 20 min at different formation potentials was examined. The passive electrode was withdrawn carefully, washed with doubly distilled water, dried and finally examined, either by X-ray diffraction or scanning electron microscopy. The data for the composition nature of the passive film formed at peak the potential of the Sb electrode (−400 mV vs SCE) confirm the existence of Sb, Sb_2O_3 as a major constituent and Sb_2O_5 as a minor one, cf. Table 3. These data support our suggestion that the peak potential of the Sb is related to the formation of Sb_2O_3/Sb_2O_5 on the electrode surface. The data obtained for Sb electrode surface treated at +1000 mV (passive region) show the existence of Sb_2O_3 and Sb_2O_5, cf. Table 4. This indicates that the Sb surface is completely covered by a thick oxide film of Sb_2O_3 and Sb_2O_5 species. In addition, there are no data from X-ray diffraction related to the presence of Sb metal in this region.

Table 3. X-ray Diffraction Pattern for Sb Surface Passivated in 0.200 M KOH Solution at Applied Potential −400 mV

Experimental values		Reported values		
dA°	I/I°	Sb	Sb_2O_3	Sb_2O_5
4.57	10	3.11	4.57	3.5
3.45	10	2.25	3.49	2.93
3.206	100	1.8	3.17	2.49
3.14	45	1.42	3.14	1.68
3.118	45	1.36	3.118	1.55
3.11	45		2.65	1.48
2.98	32		1.93	
2.77	15		1.675	
2.57	15			
2.26	25			
1.96	63			
1.74	15			
1.68	63			
1.43	16			
1.36	11			

Table 4. X-ray Diffraction Pattern for Sb Surface Passivated in 0.200 M KOH Solution at Applied Potential +1000 mV

Experimental values		Reported values	
dA°	I/I°	Sb	Sb_2O_5
4.6		4.57	3.57
3.53		3.49	2.93
3.218		3.17	2.49
2.93		3.14	1.68
2.79		2.73	1.55
2.5		1.93	1.48
1.99		1.67	
1.69			
1.43			

X-ray data for alloy Ⅱ (20% Sn), treated potentiostatically at −720 mV (peak Ⅰ), indicate that the surface contains Sb, Sn and small amounts of SnO/SnO_2, cf. Table 5. This result implies that the peak potential at −720 mV vs SCE may be attributed to tin oxide formation (SnO and SnO_2) on the alloy surface. However, the data for alloy Ⅱ, treated at −340 mV (peak Ⅱ), show that the surface is partially covered by SnO_2, Sb_2O_3 in large amounts, and Sb_2O_5 in small amounts, cf. Table 6. The data for alloy Ⅱ treated at +1000 mV (passive region), reveal that the surface is covered by the oxides SnO_2,

Table 5. X-ray Diffraction Pattern for the Passive Film on Alloy Ⅱ Surface (20% Sn) Formed Anodically in 0.200 M KOH Solution at Applied Potential −720 mV

Experimental values		Reported values			
dA°	I/I°	Sb	Sb-Sn	SbO	SnO_2
3.35	10	3.11	3.06	2.99	3.35
3.13	100	2.25	2.16	2.69	2.6
3.09	40	2.15	1.37	1.8	1.77
3.00	44	1.8		1.9	1.6
2.72	56	1.37		1.49	1.4
2.6	56				
2.26	56				
2.16	56				
1.95	5				
1.79	31				
1.77	15				
1.42	12				
1.38	11				
1.37	14				

Table 6. X-ray Diffraction Pattern for the Passive Film on Alloy Ⅱ Surface (20% Sn) Formed Anodically in 0.200 M KOH Solution at Applied Potential −340 mV

Experimental values		Reported values			
dA°	I/I°	Sb	Sb_2O_3	Sb-Sn	SnO_2
4.52	19	3.11	4.57	3.06	3.35
3.46	29	2.25	3.49	2.16	2.64
3.18	51	2.15	3.17	1.37	1.77
3.13	100	1.42	3.14		2.4
3.11	33	1.37	3.118		1.67
3.05	19				
2.72	19				
2.62	19				
2.4	8				
2.26	19				
2.16	29				
1.75	21				
1.43	29				
1.36	10				

Sb_2O_3 and Sb_2O_5, cf. Table 7.

Figure 9(a, b, c and d) shows scanning electron microscope photographs of the Sb anode surface obtained from experiments performed at different potentials (−400, 0 and +1000 mV vs SCE) for 20 min in 0.2 M KOH solution. The data shown in Fig. 9a imply that the treated surface at −400 mV (peak potential) is so completely covered by the passive oxide film that the electrode surface can not be seen. Two layers are observed on the electrode surface (double nature). The crystals of the upper layer exhibit different shapes. The crystals of this layer are not compact, i.e., there are vacancies between them. Underneath the upper layer, the second layer appears, but it seems to lie below that observed from the upper layer. These observations are in good agreement with the data of X-ray diffraction, in that the upper layer is related to Sb_2O_3, while the underneath layer is due to Sb_2O_5 formation. However, the photograph of Sb treated anodically at 0 V (more positive potential) given in Fig. 9b shows that the quantity of oxide crystals in the upper layer is less than those observed in Fig. 9a (at more negative potential) and the crystal size is smaller. The vacancies between crystals become wider, so that the crystals of the underneath layer appear easily through them. Also, the amount of crystals in the underneath layer is much greater compared with the same layer formed at −400 mV. These results support the conclusion that the amount of Sb_2O_5 crystals (underneath layer) increases at more positive potentials. In this case, the electrode surface seems to be completely covered by Sb_2O_5. For the Sb electrode surface treated at +1000 mV, Fig. 9c, it is observed that the amount of crystals in the upper layer has decreased sharply, and the distance between them has become wider compared with the crystals of the underneath layer which appear through. The quantity of oxide crystals in the underneath layer has increased and are greater in size. This indicates that Sb_2O_5 is more predominant at high anodic potentials. Accordingly, all of the above results can be explained as following: at −400 mV, the quantity of the oxide crystals in the underneath layer is small, so the crystals in the upper layer are tightly adsorbed on the bare surface of the metal. But, on imposing a more positive potential, the quantity of the oxide crystals in the underneath layer increases and they become more compact, whereas the crystals in the upper layer become loosely bound to the metal surface and dissolve into the bulk of the solution. Fig. 9d shows the different shapes of Sb oxides at +1000 mV at high magnification (7500x), where the shapes of the crystals are more clear.

Table 7. X-ray Diffraction Pattern for the Passive Film on Alloy Ⅱ Surface (20% Sn) Formed Anodically in 0.200 M KOH Solution at Applied Potential +1000 mV

Experimental values		Reported values		
dA°	I/I°	Sb_2O_3	Sb_2O_5	SnO_2
4.52	10	4.56	3.5	3.35
3.47	10	3.49	2.93	2.64
3.35	10	3.17	2.49	1.77
3.18	100	3.148	1.68	1.68
3.14	31	3.118	1.55	1.44
3.118	57	2.65	1.48	
2.94	55	1.93		
2.8	31	1.67		
2.63	10			
2.53	10			
2.24	16			
2.15	42			
1.96	33			
1.79	16			
1.67	39			
1.43	18			

Figure 10(a, b and c) shows some SEM photographs of alloy Ⅱ (20% Sn), where the anode surface is obtained from experiments performed at different anodic potentials (−400, 0 and +1000 mV vs SCE) for 20 min in 0.2 M KOH solution. The electrode surface treated anodically (at −400 mV) revealed that the surface is covered by a few Sb_2O_3 crystals and very small particles, may be of tin oxide, which are formed prior to the formation of antimony oxides on the electrode surface. However, at high positive potential (0 mV), the elec-

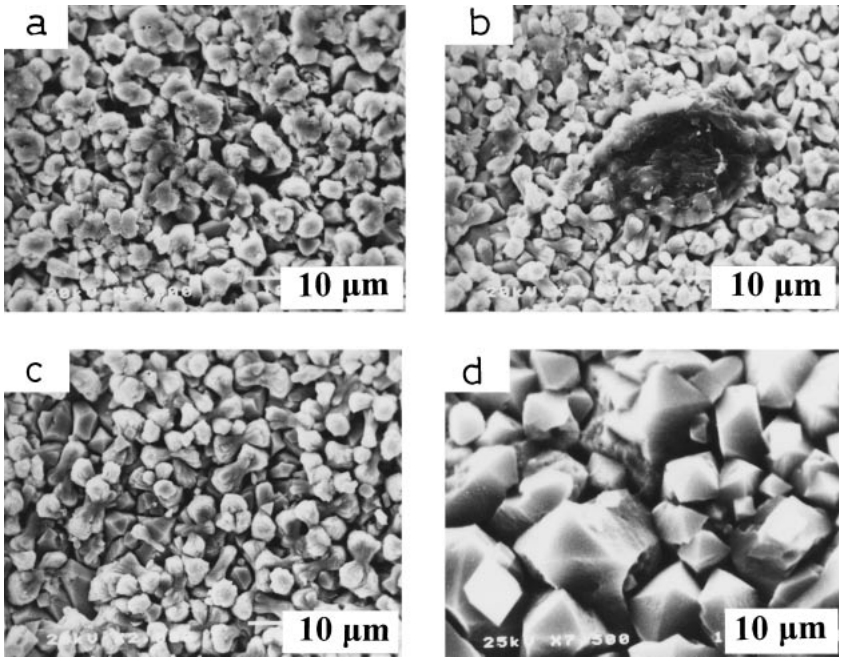

Fig. 9. SEM photographs of passive film on Sb surface formed anodically in 0.2 M KOH solution at (a) −400 mV, (b) 0 mV, (c) +1000 mV at magnification 2000× and (d) +1500 mV at magnification 7500×.

trode surface contained a greater number of crystals, which were loosely connected to each other and had large vacancies between them. The oxide crystals in the upper and underneath layer are similar to those observed in the case of Sb. The surface of the alloy treated at +1000 mV showed that the concentration of antimony oxide crystals is higher compared with the last two samples, which were treated anodically at lower anodic potentials. The particles in the upper layer are rendered closer and are much bigger in size and cover most of the electrode surface. This result suggests that the formation of Sb_2O_5 is more pronounced at high anodic potentials. The particles in the underneath layer can still be identified, but their concentration is very low. Moreover, it is suggested that the formation of tin oxides on the alloy surface retards the oxidation of Sb into Sb_2O_5.

From the discussion above, galvanostatic measurements determined both active and passivation potentials for Sb and its investigated Sn alloys. Moreover, these measurements showed how passivation potentials and passivation time were decreased by alkali conditions and Sn content in the alloy. Furthermore, potentiodynamic plots were important to index the important anodic current peaks at both active dissolution and passive potentials found in the galvanostatic results. The obtained results showed passivation potentials shifted to more negative and dissolution to more positive values, i.e., confirmed the results of the galvanostatic methods: that Sn content facilitates passivation and hinders dissolution or corrosion of the Sb electrode. Again, potentiostatic *i-t* plots indicated a delay of the active dissolution peak and its decay with increasing Sn content, cf. Fig. 7. Moreover, the current peak for passivation, i.e., the current consumed in forming oxides on Sb electrode, declines and passivation gets easier. These results support the corresponding issues deduced from both galvanostatic and potentiodynamic tests. Above all precedents, the potentiostatic passivation films prepared were examined by X-ray and electron scanning microscope to determine their compositions.

Conclusions

(1) Inhibition of active anodic dissolution and a decrease of both the passivation potential and passivation time (τ), with an increase of Sn content in the alloy, are observed.
(2) Current peak gradually decreases with increasing Sn content in the alloy compared with the current peak of pure Sb. This behaviour shows that Sn content in the Sb-Sn alloy plays an important role in decreasing the corrosion rate of Sb in alkaline solution. This behaviour indicates that the existence of Sn with Sb would enhance the corrosion resistance of antimony.
(3) Alloy Ⅳ (50% Sn) exhibited immediate passivation (potential–time curves) which may be attributed to high coverage of the surface by insoluble tin oxide.
(4) Sb showed one anodic peak, while alloys Ⅰ, Ⅱ and Ⅲ showed two anodic peaks. The first peak appeared at about −780 mV corresponding to SnO_2 and/or $Sn(OH)_2$, and the second peak at about −450 mV, corresponding to Sb_2O_3/Sb_2O_5 for alloys Ⅰ, Ⅱ and Ⅲ. In the case of alloy Ⅳ a third peak at about −940 mV is observed corresponding to the Sn/SnO charge transfer reaction.
(5) X-ray diffraction and SEM micrographs confirmed that the oxide film formed on the Sb surface in alkaline solution at different applied potentials is composed of two layers. The surface of alloy Ⅱ (20% Sn) polarized at −720 mV (peak Ⅰ) is found to contain small amounts of SnO/SnO_2 crystals, and which, at more anodic polarization potentials, is covered by SnO_2, Sb_2O_3 and Sb_2O_5.

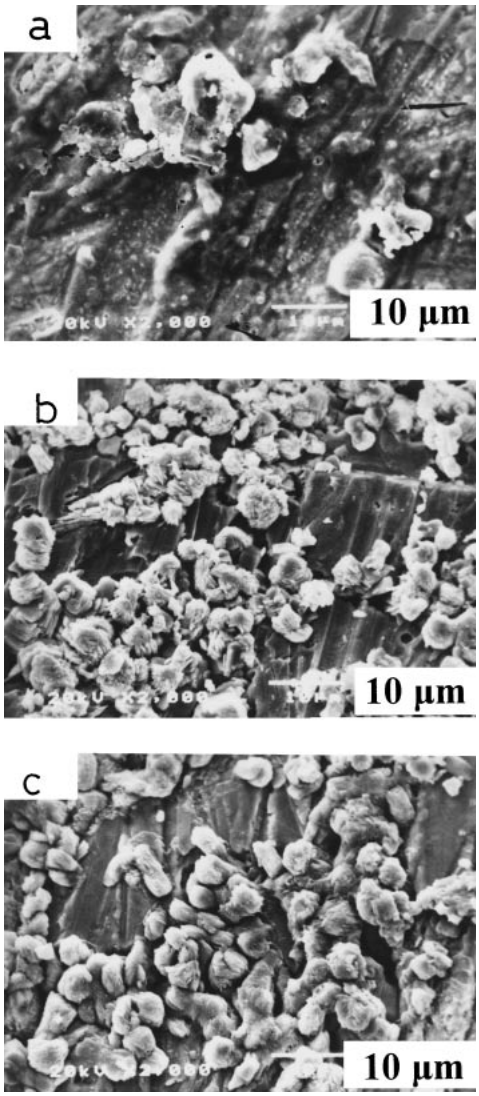

Fig. 10. SEM photographs of passive film on the alloy (II) surface formed anodically in 0.2 M KOH solution at (a) −400 mV, (b) 0 mV and (c) +1000 mV at magnification 2000×.

References

1 J. T. Stock, W. C. Purdy, and L. M. Garcia, *Chem. Rev.*, **58**, 611 (1958).

2 D. J. Ives and G. J. Janz, "Reference Electrode," Academic Press, New York (1961), p. 37, 351.

3 G. Edwell, *Electrochim. Acta*, **24**, 595, 605 (1972).

4 M. Metikos-Hukovic and B. Lovrecek, *Electrochim. Acta*, **25**, 717 (1980).

5 L. L. Wikstrom, *J. Appl. Electrochem.*, **14**, 257 (1984).

6 A. G. Gad Allah, S. A. Salih, and A. S. Mogoda, *Corrosion*, **46**, 214 (1990).

7 T. Grube and Z. Schweigardt, *Electrochem.*, **29**, 267 (1923).

8 H. C. Wu, Y. F. Shao, T. K. Chou, and M. K. Tung, *Hua Hsueh Hsueh Pao.*, **31**, 277 (1965).

9 J. Yahalom and T. P. Hoar, *Electrochim. Acta*, **15**, 877 (1970).

10 A. S. Mogoda, M. M. Hefny, and M. S. El-Basiouny, *Indian J. Technol.*, **29**, 85 (1991).

11 N. A. Darwish, A. Abdel Razik, E. M. Kairy, and T. H. Hussein, *Corros. Prev. Control*, **32**, 127 (1985).

12 N. A. Darwish, A. Abdel Razik, A. M. Mahgoub, and T. H. Hussien, *Corros. Prev. Control*, **33**, 125 (1986).

13 N. A. Darwish, A. Abdel Razik, A. M. Allam, and T. H. Hussien, *Corros. Prev. Control*, **35**, 79 (1988).

14 S. S. Abdel-Rehim, A. El-Sayed, and A. A. El-Samahi, *Surf. Coat. Technol.*, **27**, 205 (1986).

15 A. El-Sayed, *J. Appl. Electrochem.*, **27**, 193 (1997).

16 F. Sommer, R. Luck, N. Rupf-Bolz, and B. Predel, *Mater. Res. Bull.*, **18**, 621 (1983).

17 I. A. Ammar and A. Saad, *J. Electroanal. Chem.*, **34**, 159 (1972).

18 F. F. Faizullin and B. S. Mironov, *Uch. Zap. Kazan. Gos. Univ.*, **124**, 35 (1964).

19 A. A. Abdel Azim and M. M. Anwar, *Corros. Sci.*, **9**, 193 (1969).

20 W. M. Latimer, "Oxidation Potential," Prentice Hall, New York (1953).

21 A. Abdel Razik, N. A. Darwish, A. M. Allam, and T. H. Hussein, *Indian J. Chem., Sect. A*, **24**, 665 (1985).

22 A. L. Pitman, M. Pourbaix, and N. D. Zoubov, *CEBELCOR, Rapp. Tech.*, **5**, 19 (1957).

23 H. Brabre, C. Bagger, and E. Mahaan, *Electrochim. Acta*, **16**, 559 (1971).

24 D. R. Gabe and P. Stripatr, *Trans. Inst. Met. Finish.*, **51**, 141 (1973).

25 F. A. Cotton and G. Wilkinson, "Advanced Inorganic Chemistry" 3rd ed, John Wiley, Interscience, New York (1972).

26 B. N. Stirrup and N. A. Hampson, *J. Electroanal. Chem.*, **67**, 57 (1976).